Numerical 2D modeling of site response in Dinar Graben, Southwest Turkey, and comparison with observations

Esref Yalcinkaya and Omer Alptekin

Department of Geophysical Engineering, Engineering Faculty, Istanbul University, Avcilar, Istanbul, Turkey

Abstract

The October 1, 1995 Dinar earthquake (M_L=5.9) caused extensive damage within a limited area in Dinar town located in southwestern Turkey. Graben structure of the damaged area suggests the basin edge effects as a potential factor on the occurred damage. In this study numerical 2D site responses in the Dinar Graben are computed by using a finite-difference scheme and numerical results are compared with the observations within the graben. Our results suggest that the ground motions within the Dinar Graben were dominated by surface waves generated from the edges of the garben. In addition to magnifying amplitudes within the graben, the surface waves increased the duration of ground motion. Synthetic response spectra of the mainshock have shown that spectral accelerations at different sites in the graben are larger than the observed one. High spectral accelerations and long durations of ground motion may explain the extensive damage observed within the Dinar Graben.

Key words *2D modeling – basin edge effect – Dinar – site response*

1. Introduction

Amplification of seismic ground motion within sedimentary basins has long been recognized as a primary cause of damage during large earthquakes (*e.g.*, Gutenberg, 1957; Borcherdt, 1970). Basically, the impedance contrast between the bedrock and sediment layers (1D site effects) is involved in explaining the amplification of ground motion. More recently, observational and numerical studies have emphasized the importance of basin edge generated surface waves leading to increased amplifications and durations within sedimentary basins (*e.g.*, Chavez-Garcia *et al*., 1999; Raptakis *et al*., 2000). Numerical modeling has shown for a long time that such phenomena are very likely due to the generation of local surface waves by thickness variations and their trapping inside the sediment layers (Bard and Bouchon, 1980a,b). The experimental evidence of basin edge effect, first defined by Kawase (1996) as an explanation for the damage in Kobe, occurred as a result of constructive interference between the direct *S*-wave traveling up through the sediments and a basin edge generated surface wave. Direct observations of basin edge generated surface waves have been less common (*e.g.*, Field, 1996), and are usually concerned with long period surface waves propagating in large size valleys, thus they can be easily seen several tens of seconds after the *S*-wave train (*e.g.*, Kagawa *et al*., 1992; Phillips *et al*., 1993; Hatayama *et al*., 1995). In smaller structures (*i.e.*, those having lateral dimensions smaller than about 10 km), reverberating wave trains are mixed and it becomes difficult to identify locally generated surface waves

Mailing address: Dr. Esref Yalcinkaya, Department of Geophysical Engineering, Engineering Faculty, Istanbul University, 34320 Avcilar, Istanbul, Turkey; e-mail: eyalcin@istanbul.edu.tr

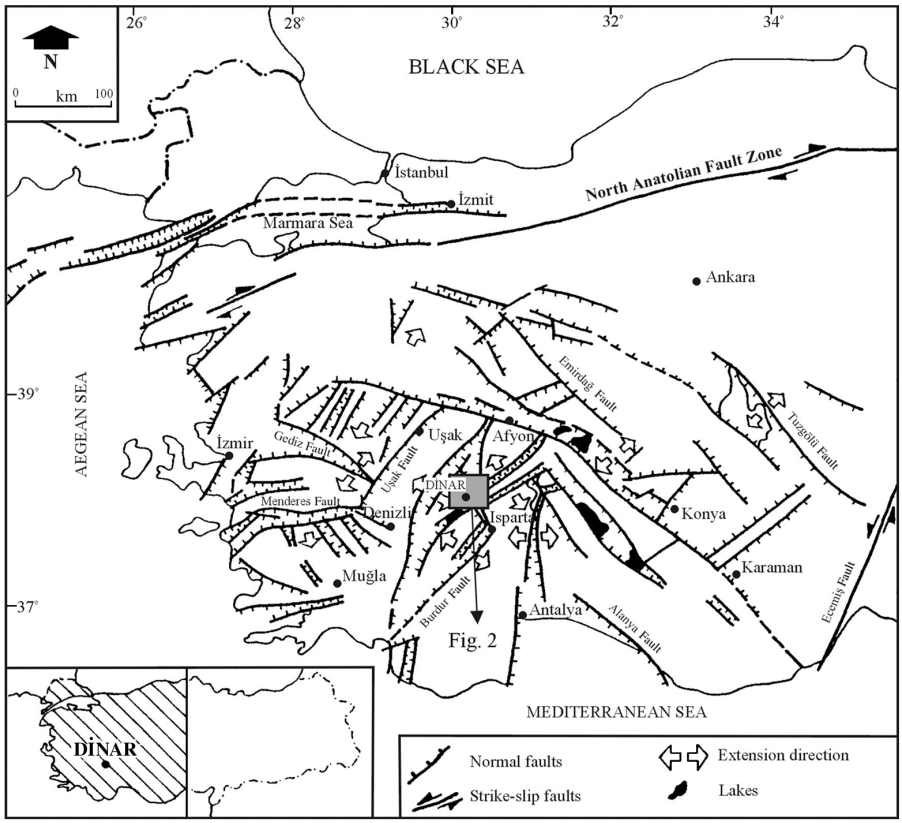

Fig. 1. Simplified tectonics map of Western Turkey (adapted from Kocyigit, 1984). The square indicates the area in fig. 2.

(Chavez-Garcia *et al*., 1999; Rovelli *et al*., 2001; Cornou *et al*., 2003a,b). The first examples of such effects are usually based on the fact that 1D modeling cannot capture the essential features of the measured response, for example amplification and duration (*e.g.*, Reipl *et al*., 2000; Makra *et al*., 2001; Triantafyllidis *et al*., 2001). In case of a complex subsurface geometry at least 2D modeling is mandatory in site effects estimation.

The Dinar Graben, which is located in the Southwestern Turkey and has dominantly extensional tectonic regime, is chosen as the study area (fig. 1). The Dinar Graben extends SE-NW, ranging in width from 1.5 km in the SE to 15 km in the NW portion. The Dinar Fault is about 75 km long and strikes NW-SE direction bordering northeast side of the Dinar Graben. It has normal fault characteristics dipping in the NW direction with the downthrown western block and the upthrown eastern block. In response to this, the western block is a graben (Dinar Graben) and the eastern block is a horst (Akdag Horst) (fig. 2). The Dinar Graben is very young (Plio-Quaternary) and filled with thick (nearly up to 200 m) unconsolidated sedimentary deposits (gravel, sand, silt, clay), whereas the Akdag Horst is comprised of old, more stable rock formations (limestone, conglomerates) (Kocyigit, 1984; Kayabali, 1997; Durukal *et al*., 1998). October 1, 1995 Dinar earthquake (M_L=5.9) occurred on the Dinar

Fault and caused 92 deaths in Dinar town and nearby villages. Dinar town is located at the east edge of the Dinar Graben (fig. 2), and settlement is mostly on alluvium and partly on hills. Damage was strikingly concentrated within a limited area over the alluvium and adjacent to the rock outcrop (Ansal *et al*., 2001; Bakir *et al*., 2002; Sucuoğlu *et al*., 2003). Previous studies (Kayabali, 1997; Ersahin, 1998) based on 1D models have failed to explain this discrepancy in the distribution of the observed damage. Yalcinkaya and Alptekin (2005) examined the time and frequency domain characteristics of weak motion records recorded at stations located in and out the Dinar Graben. They have emphasized that basin edge surface waves have important contributions on amplitudes and durations of the records within the graben.

This study aims a 2D numerical modeling of the Dinar Graben based on a finite-difference scheme (Zahradnik *et al*., 1994; Zahradnik, 1995; Zahradnik and Priolo, 1995), and comparing with the results of an experimental study carried out by Yalcinkaya and Alptekin (2005). A second aim of this paper is to investigate the extent of the role of basin effects on the observed degrees and distribution of damage in Dinar.

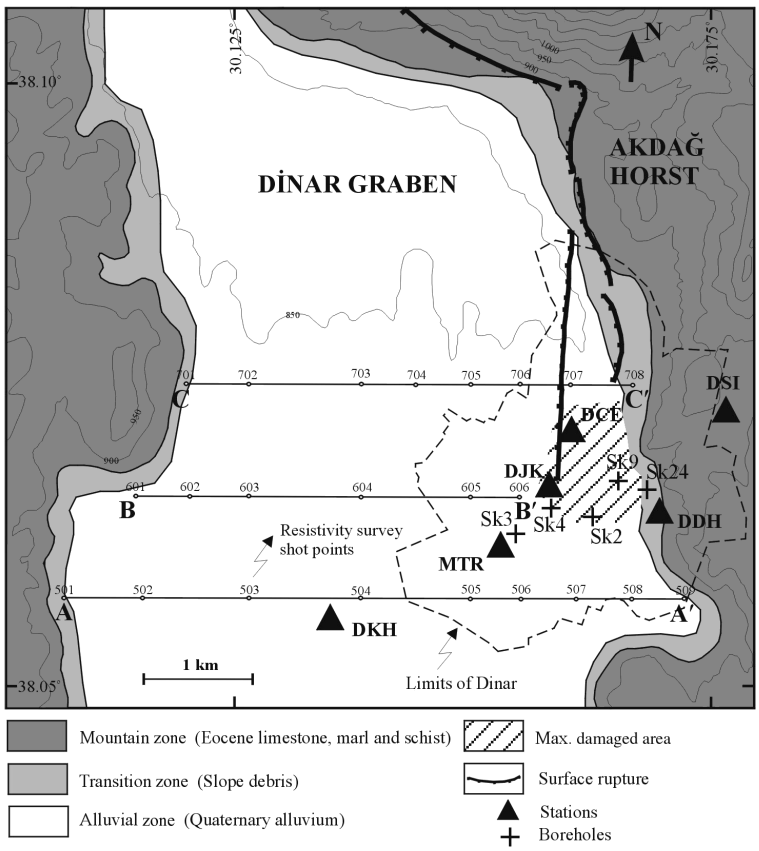

Fig. 2. Geological map of the Dinar Graben and its vicinity. Triangles indicate the recording stations used in this study. A-A′, B-B′ and C-C′ are the locations of resistivity profiles shown in fig. 3. + presents the locations of the boreholes shown in fig. 4.

2. Structure of the Dinar Graben

The first study made to define the structure of the Dinar Graben is a geophysical resistivity survey along E-W axis (Ozpinar, 1978). This is only study aimed to expose the bedrock structure underlying the Dinar Graben. After the October 1, 1995 Dinar earthquake these data were re-interpreted by Turker *et al*. (1996) and Kayabali (1997). Typical cross-sections obtained from this survey are shown in fig. 3. These sections show that depth of the bedrock within the graben changes significantly both in EW and NS directions. At some points in the graben, thickness of the sediments exceeds 200 m. After the Dinar earthquake of October 1, 1995 extensive geotechnical investigations were performed in and around Dinar (Turker *et al*., 1996; Sucuoğlu *et al*., 1997; Erken *et al*., 1999; Gullu, 2002). These include numerous 20-40 m deep boreholes opened in different points of the town. Standard Penetration Tests (SPT) were performed at the borehole sites and down-hole tests were made at two points. A sample cross-section obtained from the boreholes is shown in fig. 4. *P*- and *S*-wave velocity profiles obtained from down-hole test site at Sk3 are shown in fig. 5. In addition, seismic refraction tests were performed at many profiles, but, penetration depths of these tests were very shallow (maximum 20 m). Only deep investigation is water wells reaching 100 and 163 m previously opened in the graben approximately 2 km southwest of the town. Clay cemented conglomerate was observed to underlie the alluvium from both logs at near 100 m depth, which persisted to the end of log in the case of deeper well (Bakir *et al*., 2002).

According to the information obtained from these boreholes, the geologic strata in the Dinar Graben are composed of clay/clayey sand/gravel/gravely sandy clay from the surface to the basement. The groundwater level varies between 1-5 m. To construct a reliable model of the geological structure, our prior interests are to know the shear wave velocities, the sediment-bedrock interface and possible lateral variations within the graben. Despite many studies per-

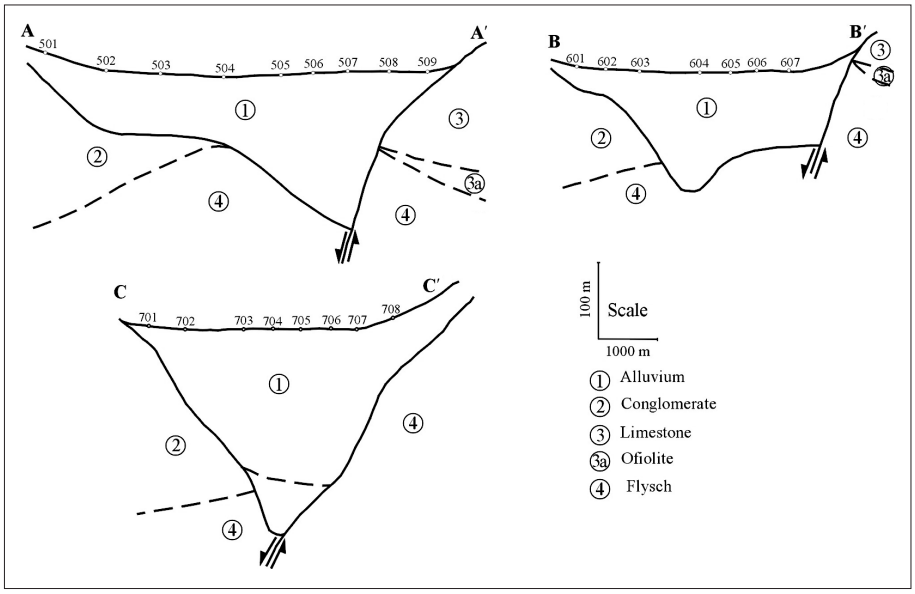

Fig. 3. E-W cross-sections across the Dinar Graben determined from the resistivity tests shown in fig. 2 (after Ozpinar, 1978; Turker *et al*., 1996; Kayabali, 1997).

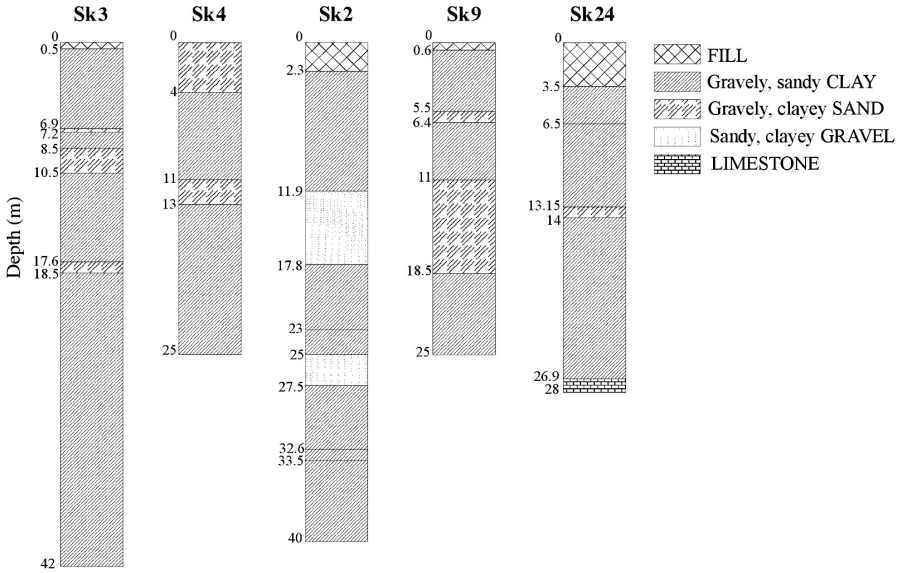

Fig. 4. Boreholes showing typical soil formations in the Dinar Graben. Locations of the boreholes are shown in fig. 2 (after Gullu, 2001).

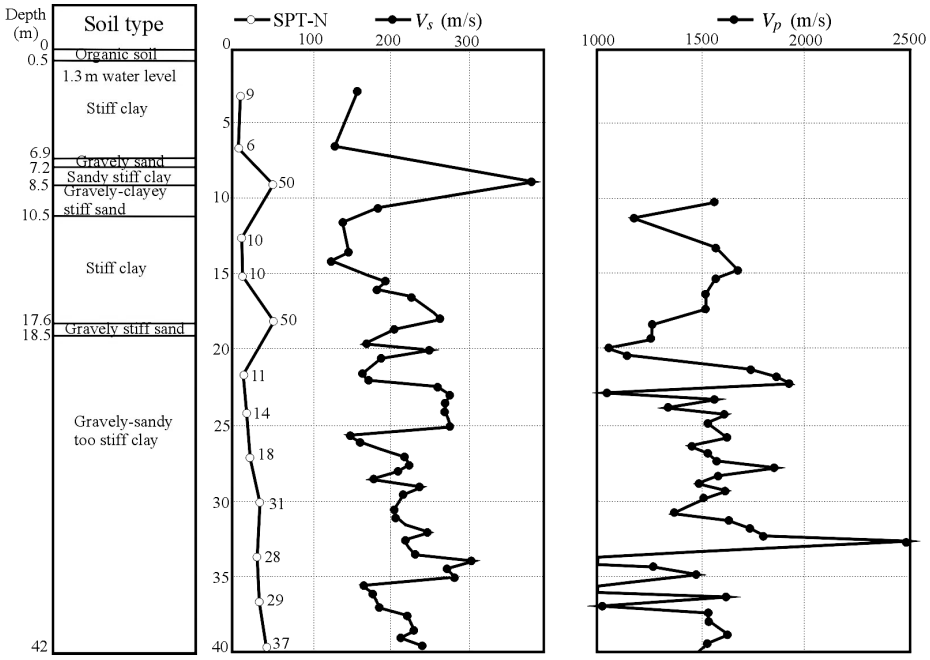

Fig. 5. Depth-section and physical parameters obtained by down-hole test at Sk3 borehole (after Gullu, 2001).

formed in the area, unfortunately these data are not well known. Especially there is no information on deep shear velocity structure. Therefore, several hypothetical cross-sections were drawn synthesizing the extrapolated data derived from the aforementioned studies, and they were tested in order to construct the most reliable model. The final model is shown in fig. 6. This model approximately describes the structure in E-W direction near the B-B′ cross-section shown in fig. 2, and it is certainly too simplified, when borehole results are taken into account. In addition, this profile centers Dinar town, the boreholes and the stations. The model consists of ten blocks, which are composed of four different formations. Physical parameters of each block are given in table I. To define some parameters (attenuation or shear wave velocity), especially for deep formations within the graben, information from similar geologic structures, *e.g.*, the Volvi Graben (Euroseistest site: Chavez-Garcia *et al*., 2000; Raptakis *et al*., 2000), was considered. Formation 1 consists of gravely-sandy clays, is a recent loose deposit. Formation 2 is composed of more stiff clayey-silty sands and sandy clays. Formation 3 corresponds weathered rock and slope debris. Transitions among these three formations within the graben are irregular in realty, however, we use quite smooth borders between these formations, because our knowledge is insufficient and the model is defined with limited number of blocks with limited dimensions. Finally, formation 4 is the bedrock, which is largely composed of flysh-type formations of Eocene Age, and conglomerates of Oligocene Age.

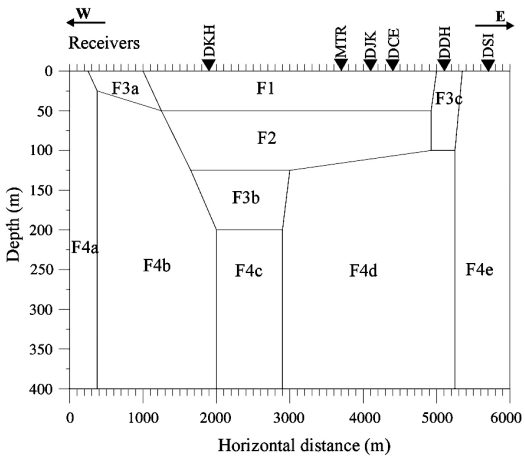

Fig. 6. Final model adjusted for the application of 2D finite-difference modeling. The model is drawn on E-W direction near the B-B′ cross-section shown in fig. 2. Observation stations projected on the cross-section are shown with triangles. The physical parameters for each block are given in table I.

Table I. Physical parameters of the blocks used in the 2D finite-difference modeling.

Block number (see fig. 6)	*S*-wave velocity (v_s) (m/s)	Density (ρ) (kg/m^3)	Quality factor (Q_s)
F1	300	1900	30
F2	450	2100	45
F3a-F3c	700	2100	70
F4a-F4e	2300	2600	230

3. 2D modeling

The faults bordering the Dinar Graben are nearly in NS direction. Therefore, it is considered that the surface waves are mainly generated from these faults located in the east and the west of graben, and they propagate mainly in E-W direction within the graben. In this paper, we have limited ourselves to site effects evaluated in the horizontal component directed along the long axis of the graben (NS component), perpendicular to fig. 6 (SH motion). The surface waves in this component consist of mainly Love waves. The in-plane component (SV motion for Rayleigh waves) will be the subject of another study. The 2D response of the model of fig. 6 was computed applying the finite-difference scheme (Zahradnik *et al*., 1994; Zahradnik, 1995; Zahradnik and Priolo, 1995). The surface displacement is calculated by the propagation of an incident plane wave across the finite-difference grid applying the basic equations at all grid points. The surface is considered to be flat, and

the near-subsurface structure is adjusted on the geophysical model by convex polygons with constant velocity (v_s), density (ρ) and quality factor (Q_s). The wave field is strongly attenuated at the borders to eliminate parasitic reflections from the borders of the model.

We used a constant grid step of 5 m in the horizontal and vertical directions. We chose a maximum accurate frequency of 6 Hz for our computations, covering the main amplification peaks determined in Yalcinkaya and Alptekin (2005). This means 10 grid points per shortest *S*-wavelength corresponding to a frequency of 6 Hz. Given a minimum shear wave velocity of 300 m/s (formation 1 of the model), our minimum wavelength is 50 m. In addition, this frequency limitation is justified that there is not enough detailed knowledge on the geological structure in the Dinar Graben to have confidence in higher frequency simulations. Attenuation is taken into account by Q values, which are assumed to be valid at 1 Hz. Time steps of simulation are 0.001 s, and total length of the time series is 10 s. For the excitation from below, a vertically incident plane *SH*-wave is used with a Ricker wavelet with duration $T_0 = 0.5$ s.

4. Comparison of synthetic and observed seismograms

Figure 7 shows the displacement time histories of 61 receivers distributed every 100 m along the free surface of the 2D soil profile. They have been low-pass filtered at 6 Hz. The most important feature of the synthetic seismograms is the surface wave trains generated at east and west borders of the graben. These surface waves converge towards the center of the graben, resulting in large amplitudes lasting for more than 6 s, in large contrast with ground motion duration outside the central part of the graben. The receivers at the center of the graben show the 1D resonance of the sediments, and their amplitudes attenuate very fast. The Love waves generated from the edges have the largest amplitudes at the receivers near the edges of the graben. While toward to the center of the graben the durations increase, the amplitudes are not so high. Because the slope at the east edge of the graben is higher than that of the west edge, the surface waves are effective in shorter distance (between DDH and DJK, nearly 1 km) at the east side relative to the west side.

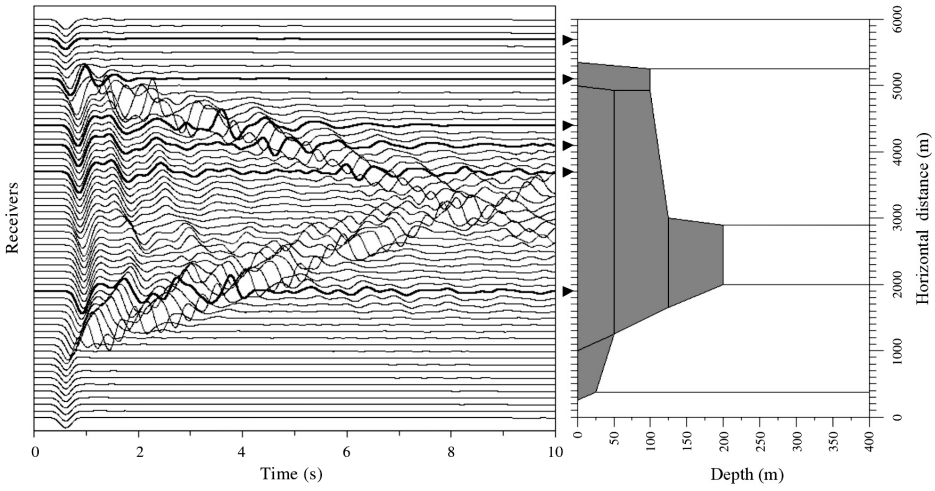

Fig. 7. Time histories computed by 2D finite difference modeling for vertical incidence of *SH*-waves. The model and observation stations have been indicated on the right for reference. Time signals matching with the observation stations are shown with thick traces. All traces have been low-pass filtered at 6 Hz.

This result coincides with the high damage which occurred in that area.

After the October 1, 1995 Dinar earthquake, a small temporary network of 5 three-component stations (DKH, DJK, DCE, DDH and DSI in fig. 2) operated in the Dinar Graben. Yalcinkaya and Alptekin (2005) estimated average amplification functions at these stations, by choosing the DSI station as reference site, using the Standard Spectral Ratio method (Borcherdt, 1970). Detailed discussion concerning the experimental data and the resulting of amplification functions are given in Yalcinkaya and Alptekin (2005). We will use their NS component amplification functions for comparing our results from numerical modeling. MTR station was installed before the Dinar earthquake and recorded the mainshock (fig. 2). Unfortunately, this station did not record the same events as the temporary stations. Therefore, we estimated the amplification function at the MTR station dividing the spectrum of NS component of the mainshock (out-plane *SH* motion) to the spectrum of vertical component (the Horizontal-to-Vertical Spectral Ratio method: Lermo and Chavez-Garcia, 1993). Empirical stations do not take place along a line in the graben, therefore, they are projected on the 2D cross-section and the re-

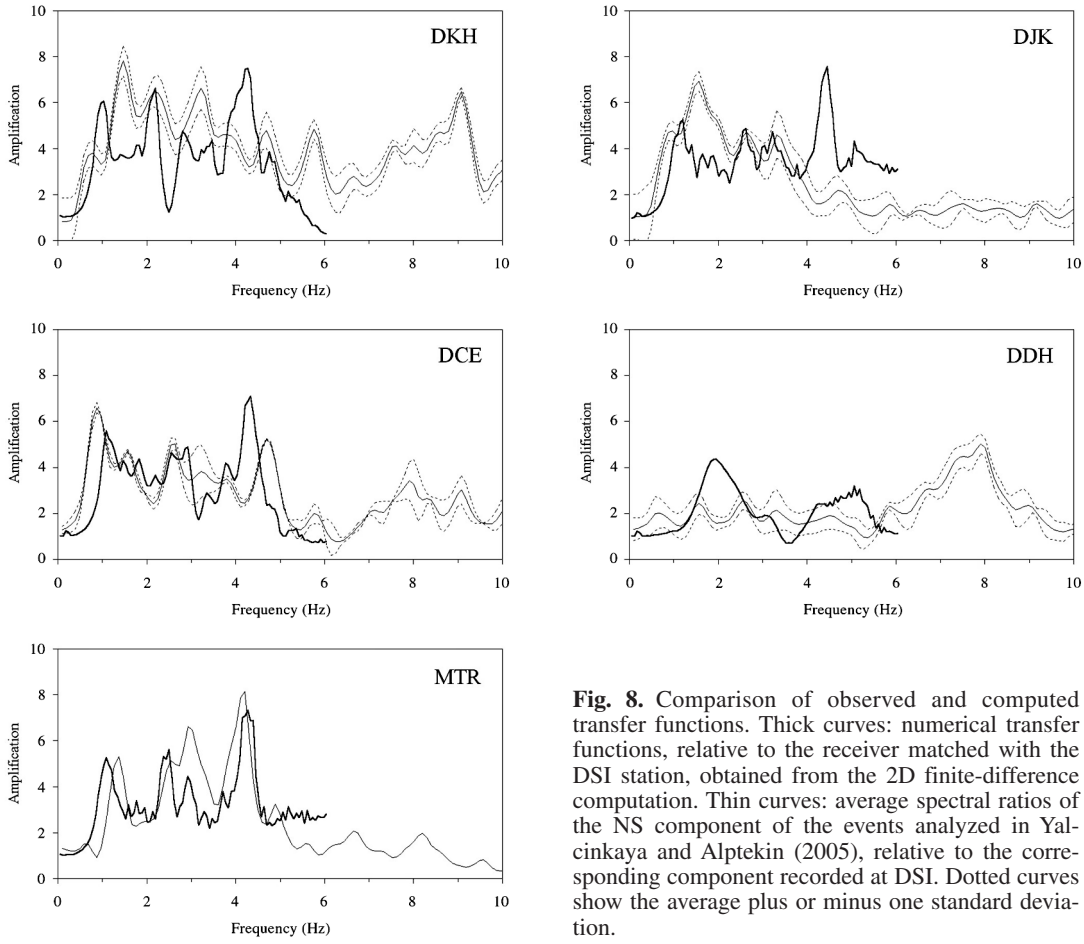

Fig. 8. Comparison of observed and computed transfer functions. Thick curves: numerical transfer functions, relative to the receiver matched with the DSI station, obtained from the 2D finite-difference computation. Thin curves: average spectral ratios of the NS component of the events analyzed in Yalcinkaya and Alptekin (2005), relative to the corresponding component recorded at DSI. Dotted curves show the average plus or minus one standard deviation.

ceiver matched with each station is defined (fig. 6). If the numbering of receivers starts from the west, the DKH, MTR, DJK, DCE, DDH, DSI stations match with the receivers 20, 38, 42, 45, 52 and 58 respectively (fig. 6). Transfer functions of the synthetics at the receivers matched with each station located inside the graben, relative to the synthetic at the receiver matched with the DSI station, are presented with thick curves in fig. 8. In fig. 8, thin and dotted curves indicate the NS component empirical average transfer function and the average plus or minus one standard deviation respectively.

At first glance, the fit between synthetics and observations is satisfying, even if several disagreements are noted, when examining more thoroughly. At DCE and MTR stations the fit is good both on the amplifications and at the peak frequencies. At DKH and DJK stations the level of amplification is well predicted, but the precise locations of peaks and troughs are missed. At the DDH station the modeled amplification curve compares poorly with the observed curve.

One of the main reasons for disagreement between the synthetics and observations may be projecting the stations on a 2D profile. Even if the 2D profile centers the stations, the projection distances may cause to uncertainties at sites like the Dinar Graben, where the stratigraphy changes at very short distances. In addition, the shape of the 2D cross section varies along the graben, and this may cause uncertainties in the comparisons. The other reason is that the 2D modeling for the Dinar Graben may be insufficient, because the returning of the faults to NW, towards north, may cause the surface waves generated from the north edge, and this requires a 3D numerical simulation.

We now compare the observed and the synthetic seismograms in the time domain. For this, we use the event of October 11, 1995 (M_L=4.1) recorded by the temporary network (Yalcinkaya and Alptekin, 2005). Figure 9a shows the NS component accelerograms of the event (*SH* motion), and fig. 9b shows the synthetic accelerograms obtained by convolution of the observed record at DSI with the corresponding 2D transfer function at each location. All traces have been low-pass filtered with a cutoff frequency of 4 Hz in order to reveal the contribution of locally generated surface waves. As seen in fig. 9a, the seismograms recorded at the stations inside the graben (DKH, DJK and DCE) have larger amplitudes and longer durations than the others recorded on the edge (DDH) and outside (DSI) of the graben. These characteristics are well reproduced by the synthetic seismograms shown in fig. 9b. The direct *S*-wave amplitudes are underestimated by the numerical 2D modeling probably due to the impedance ratio between the sediment and the basement was predicted smaller than true. The relatively large amplitude surface wave arrivals following the direct *S*-wave can be seen clearly on the synthetics inside the graben, while they are ambiguous on the observations. The attenuation accepted for the sediments in the graben may be high in realty or the destructive interferences be-

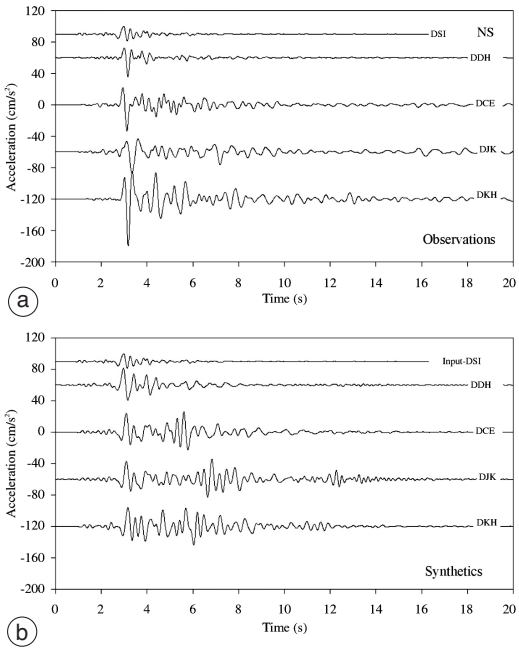

Fig. 9a,b. Comparison of synthetic and observed seismograms in the time domain for the event occurred on October 11, 1995 (M_L=4.1): a) accelerograms recorded by the temporary network; b) synthetic accelerograms obtained by convolution of the observed record at DSI with the corresponding 2D transfer function at each location. All traces have been low-pass filtered with a cutoff frequency of 4 Hz.

tween waves may not have been completely predicted by 2D modeling. In addition, in similar small structures it was observed that reverberating wave trains are mixed and it becomes difficult to identify locally generated surface waves (Cornou *et al*., 2003a,b). As emphasized by Yalcinkaya and Alptekin (2005), contrary to Love waves, Rayleigh waves on the EW and vertical components can be discerned easily.

Figures 8 and 9a,b show that the agreement between synthetic and observation is not very good at some stations, because the geological structure and material properties of the Dinar Graben are known poorly, and the data are inconvenient in order to make a detailed comparison. A 3D or more accurate 2D velocity structure may explain better some inconsistencies between the synthetic and observed seismograms. However, the results show that the surface waves are very important on the records especially near the edges of the graben, where the severe damage occurred during the Dinar earthquake.

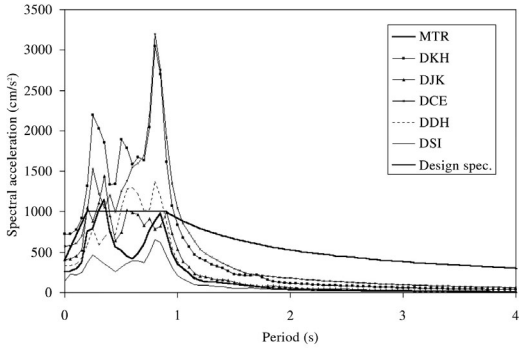

Fig. 10. Comparison of the 5% damped synthetic response spectra with the observed response spectra at MTR for the Dinar earthquake, and the elastic design spectra defined in the Turkish code for similar seismic zone and soil characteristics. Reference base motion for the synthetics was obtained by deconvolution of the mainshock at MTR station with the corresponding 2D transfer function for this station, and then the base motion was convoluted with the corresponding transfer function at each location for the surface motions.

5. Simulations of the mainshock response spectra

In this part of our study, we will simulate the mainshock records of the Dinar earthquake at the receivers matched with the temporary network stations. Reference base motion was obtained by deconvolution of the NS component accelerogram of the mainshock recorded at the MTR station with the corresponding 2D transfer function for the receiver 38. Synthetic surface motions were obtained by convolution of the reference base motion with the corresponding 2D transfer function at each location. Calculated response spectra with 5% damping, which are crucial for assessing the building damage, are compared with the elastic design spectra proposed by the national building code (Ministry of Reconstruction and Settlement, 1997) (fig. 10). Response spectrum of the MTR station was calculated from the NS component accelerogram of the mainshock. Dinar is located in seismic zone 1 (most severe) in the Turkish seismic zones map. The effective peak acceleration assigned to zone 1 in the Turkish national building code is 0.40 g. As seen in fig. 10, the response spectra obtained from the synthetic mainshock records, except for the DSI, are larger than the design response spectrum specified in the Turkish seismic design code. At the DKH and DCE stations, spectral accelerations are bigger three times at around 0.8 s than the others. The maximum spectral accelerations are seen at between 0.3 s and 0.8 s. This period interval corresponds to the period range of 3-8 story buildings. Maximum damage in Dinar was observed roughly between the receiver 38 and the receiver 52 on the cross-section (fig. 6), that is, between the MTR and DDH stations, and mainly 4-6 story buildings were damaged. This may explain the observed distribution of damage in Dinar. Building density is very low vicinity of the DKH or receiver 20, therefore, it could not be compared with the damage, despite the observed high amplitudes.

6. Conclusions

In this study we tried to evaluate numerical 2D modeling of site response in Dinar Graben. Because the subsurface structure in the Dinar

Graben is not known in greater details, the results do not allow a detailed comparison. The agreement between computed and observed data is not satisfactory at some stations. To explain inconsistencies between the synthetics and observations, there is a need for a 3D modeling or more accurate 2D velocity structure, as well as more exhaustive comparisons between numerical and experimental data, because the geological structure of the Dinar Graben shows important differentiations in small scales.

Despite all deficiencies, the 2D modeling shows that the ground motions inside the graben have been significantly dominated by the surface waves generated from the edges of the graben. The surface waves, by adding to *S*-waves, have increased the duration of the records within the graben. The important effects are seen at sites near the edges, where maximum damage was observed during the Dinar earthquake of 1995. Synthetic response spectra of the October 1, 1995 Dinar earthquake show high amplitudes relative to the design response spectrum specified in the Turkish seismic design code. High spectral accelerations are observed between the periods of 0.3 and 0.8 s, while maximum damaged buildings in Dinar are 4-6 stories, which have 0.4-0.6 s typical periods. Long durations and high spectral accelerations inside the graben may explain the extensive damage observed in Dinar. One limitation of our study, which must be taken into account, is that all our computations are based on the linear soil behavior.

Acknowledgements

We would like to thank Prof. J. Zahradnik for kindly providing us with the 2D finite-difference code. We are grateful to the anonymous reviewers for comments leading to an improved manuscript.

REFERENCES

ANSAL, A.M., R. IYISAN and H. GULLU (2001): Microtremor measurements for the microzonation of Dinar, *Pure Appl. Geophys.*, **158**, 2525-2541.

BAKIR, B.S., M.Y. OZKAN and S. CILIZ (2002): Effects of basin edge on the distribution of damage in 1995 Dinar, Turkey earthquake, *Soil Dyn. Earthquake Eng.*, **22**, 335-345.

BARD, P.-Y. and M. BOUCHON (1985a): The seismic response of sediment-filled valleys, Part 1. The case of incident *SH*-waves, *Bull. Seismol. Soc. Am.*, **70**, 1263-1286.

BARD, P.-Y. and M. BOUCHON (1985b): The seismic response of sediment-filled valleys, Part 2. The case of incident *P*- and *SV*-waves, *Bull. Seismol. Soc. Am.*, **70**, 1921-1941.

BORCHERDT, R.D. (1970): Effects of local geology on ground motion near San Francisco Bay, *Bull. Seismol. Soc. Am.*, **60**, 29-61.

CHAVEZ-GARCIA, F.J., W.R. STEPHENSON and M. RODRIGEZ (1999): Lateral propagation effects observed at Parkway, New Zealand: a case history to compare 1D *versus* 2D site effects, *Bull. Seismol. Soc. Am.*, **89**, 718-732.

CHAVEZ-GARCIA, F.J., D. RAPTAKIS, K. MAKRA and K. PITILAKIS (2000): Site effect at Euroseistest-II. Results from 2D numerical modeling and comparison with observations, *Soil Dyn. Earthquake Eng.*, **19**, 23-39.

CORNOU, C., P.-Y. BARD and M. DIETRICH (2003a): Contribution of dense array analysis to the identification and quantification of basin-edge-induced waves, Part I. Methodology, *Bull. Seismol. Soc. Am.*, **93**, 2604-2623.

CORNOU, C., P.Y. BARD and M. DIETRICH (2003b): Contribution of dense array analysis to the identification and quantification of basin-edge-induced waves, Part II. Application to Grenoble Basin (French Alps), *Bull. Seismol. Soc. Am.*, **93**, 2624-2648.

DURUKAL, E., M. ERDIK, J. AVCI, O. YUZUGULLU, Y. ALPAY, B. AVAR, V. ZULFIKAR, T. BIRO and A. MERT (1998): Analysis of the strong motion data of the 1995 Dinar, Turkey earthquake, *Soil Dyn. Earthquake Eng.*, **17**, 557-578.

ERKEN, A., R. IYISAN, R. OZAY and H. GULLU (1999): 1995 Dinar depreminde Dinar'da yerel zemin kosullari ve zemin davranislari, *ITU Gelistirme Vakfi*, *Teknik Rapor No. 203*, Istanbul (in Turkish).

ERSAHIN, B. (1998): Assessment of the local soil conditions on earthquake damage distribution: a case study on 1st October Dinar earthquake, *MS Thesis* (Department of Civil Engineering, Middle East Technical University), pp. 141.

FIELD, E.H. (1996): Spectral amplification in a sediment-filled valley exhibiting clear basin-edge-induced waves, *Bull. Seismol. Soc. Am.*, **86**, 991-1005.

GULLU, H. (2001): Dinar'in zemin buyutmelerine göre cografik bilgi sistemleri ile mikrobolgelenmesi, *PhD. Thesis* (Civil Engineering, Istanbul Technical University), pp. 289 (in Turkish).

GUTENBERG, B. (1957): Effects on ground on earthquake motion, *Bull. Seismol. Soc. Am.*, **47**, 221-250.

HATAYAMA, K., K. MATSUNAMI, T. IWATA and K. IRIKURA (1995): Basin-induced lowe waves in the eastern part of the Osaka Basin, *J. Phys. Earth*, **43**, 131-155.

KAGAWA, T., S. SAWADA and Y. IWASAKI (1992): On the relationship between azimuth dependency of earthquake ground motion and deep basin structure beneath the Osaka plain, *J. Phys. Earth*, **40**, 73-83.

KAYABALI, K. (1997): The role of soil behavior on damage caused by the Dinar earthquake (Southwestern Turkey) of October 1, 1995, *Environ. Eng. Geosci.,* **III**, 111-121.

KAWASE, H. (1996): The cause of the damage belt in Kobe: «the basin-edge effect». Constructive interference of the direct *S*-wave with the basin-induced diffracted/ Rayleigh waves, *Seismol. Res. Lett.*, **67**, 25-34.

KOCYIGIT, A. (1984): Guneybati Turkiye ve yakin dolayinda levha içi yeni tektonik gelisim, *Turk. Jeol. Kurumu Bul.*, **27**, 1-16 (in Turkish).

LERMO, J. and F.J. CHAVEZ-GARCIA (1993): Site effect evaluation using spectral ratios with only one station, *Bull. Seismol. Soc. Am.*, **83,** 1574-1594.

MAKRA, K., D. RAPTAKIS, F.J. CHAVEZ-GARCIA and K. PITILAKIS (2001): Site effects and design provisions: the case of Euroseistest, *Pure Appl. Geophys.*, **158**, 2349-2367.

MINISTRY OF RECONSTRUCTION AND SETTLEMENT (1997): *Seismic Code for Building in Disaster Areas*, Ankara, pp. 85.

OZPINAR, B. (1978): Geophysical resistivity investigation report on the Afyon-Dinar plain, in *18th District of the State Hydraulic Works*, Isparta, Turkey, pp. 8 (in Turkish).

PHILLIPS, W.S., S. KINOSHITA and H. FUJIWARA (1993): Basin-induced love waves observed using the strong-motion array at Fuchu, Japan, *Bull. Seismol. Soc. Am.*, **83**, 64-84.

RAPTAKIS, D., F.J. CHAVEZ-GARCIA, K. MAKRA and K. PITILAKIS (2000): Site effects at Euroseistest-I. Determination of the valley structure and confrontation of observations with 1D analysis, *Soil Dyn. Earthquake Eng.*, **19**, 1-22.

REIPL, J., J. ZAHRADNIK, V. PLICKA and P.-Y. BARD (2000): About the efficiency of numerical 1D and 2D modelling of site effects in basin structures, *Pure Appl. Geophys.*, **157**, 319-342.

ROVELLI, A., L. SCOGNAMIGLIO, F. MARRA and A. CASERTA (2001): Edge-diffracted 1-s surface waves observed in a small-size intramountain basin (Colfiorito, Central Italy), *Bull. Seismol. Soc. Am.*, **91**, 1851-1866.

SUCUOĞLU, H., J.G. ANDERSON and Y. ZENG (2003): Predicting intensity and damage distribution during the 1995 Dinar, Turkey, earthquake with generated strong motion accelerograms, *Bull. Seismol. Soc. Am.*, **93**, 1267-1279.

TRIANTAFYLLIDIS, P., P.M. HATZIDIMITRIOU and P. SUHADOLC (2001): 1D theoretical modeling for site effect estimations in Thessaloniki: comparison with observations, *Pure Appl. Geophys.*, **158**, 2333-2347.

TURKER, E., M.A. KAYA, Z. KAMACI, O. UYANIK, N. BUYUKKOSE, M. MUTLUTURK, A. YALCIN and F. OZKAN (1996): Dinar afet bolgesi geoteknik raporu, *Afet Isleri Genel Mudurlugu-Suleyman Demirel Universitesi* (in Turkish).

YALCINKAYA, E. and O. ALPTEKIN (2005): Contributions of the basin edge induced surface waves to site effect in the Dinar Basin, Southwestern Turkey, *Pure Appl. Geophys.*, **162**, 931-951.

ZAHRADNIK, J. (1995): Simple elastic finite difference scheme, *Bull. Seismol. Soc. Am.*, **85**, 1879-1887.

ZAHRADNIK, J. and E. PRIOLO (1995): Heterogeneous formulations of elastodynamic equations and finite-difference schemes, *Geophys. J. Int.*, **120**, 663-676.

ZAHRADNIK, J., J. O'LEARY and J.S. SOCHACKI (1994): Finite-difference schemes for elastic waves based on the integration approach, *Geophysics*, **59**, 928-937.

(received April 23, 2004;
accepted December 22, 2004)